A Statistical Estimate of Errors in the Calculation of Radio-Occultation Bending Angles Caused by a 2D Approximation of Ray Tracing and the Assumption of Spherical Symmetry of the Atmosphere

X. ZOU

The Florida State University, Tallahassee, Florida

HUI LIU

The Florida State University, Tallahassee, Florida, and LASG, Institute of Atmospheric Physics, CAS, Beijing, China

R. A. ANTHES

University Corporation for Atmospheric Research, Boulder, Colorado

ABSTRACT

Atmospheric data from National Centers for Environmental Prediction (NCEP) analyses and orbital parameters from 133 real Global Positioning System (GPS) meteorological data soundings are used to compute the ''true'' bending angle profiles using an accurate 3D ray-tracing procedure. They are then compared with approximate profiles obtained using the spherical symmetry assumption and an efficient 2D ray-tracing model. The average fractional error of the bending angles due to the spherical symmetry assumption is less than 0.15%. The average fractional error due to the use of the 2D ray-tracing model is slightly greater than that due to the spherical symmetry assumption. The vertical error correlations due to the spherical symmetry assumption are sharp between 6 and 8 km and broader above and below this layer. The vertical error correlations associated with the 2D forward model show a nearly diagonal structure below 15 km with high correlation confined to a 2-km layer centered at the observation level.

1. Introduction

The Global Positioning System/Meteorology (GPS/MET) experiment (Ware et al. 1996; Kursinski et al. 1996; Rocken et al. 1997) demonstrated the feasibility of obtaining accurate soundings of the ionosphere and the neutral atmosphere using the radio occultation technique. Although the number of global soundings produced by the one satellite in the GPS/MET experiment was very small, the Constellation Observing System for Meteorology, Ionosphere and Climate (COSMIC) experiment plans to launch six GPS receivers in 2005, providing approximately 3000 soundings globally per day [see Lee et al. (2001) for an extensive description of the radio occultation technique, the GPS/MET experiment, and COSMIC]. In preparation for COSMIC and other future satellites that will produce radio occultation soundings, it is important to develop accurate and computationally efficient methods of assimilating these data in NWP models and to demonstrate the usefulness of these occultation data using observations obtained in the GPS/MET experiment.

The radio occultation method is described in many places (e.g., Eshleman 1973; Kursinski et al. 1997; Rocken et al. 2001; Kursinski et al. 2001; Kuo et al. 2001) and so we provide only a brief summary here. In a GPS occultation, a GPS receiver on a (low earth orbiting) (LEO) satellite tracks the occulted radio wave signals (at two frequencies) as a GPS satellite rises or sets behind the earth (Fig. 1). The electron density in the ionosphere and density in the neutral atmosphere cause the radio waves to be slowed and refracted. From the measured Doppler-shifted frequencies on the LEO, the positions and vector velocities of the LEO and GPS satellites, and the assumption of spherical symmetry of the atmospheric density, it is possible to obtain the bending angle α as a function of impact parameter a (see Fig. 1 for the relevant geometry and an illustration of α and a).

Given $\alpha(a)$ and using the spherical symmetry assumption again, the vertical profile of atmospheric refractivity N can be obtained using an Abel transform

Corresponding author address: Dr. X. Zou, Department of Meteorology, The Florida State University, 404 Love Building, Tallahassee, FL 32306.
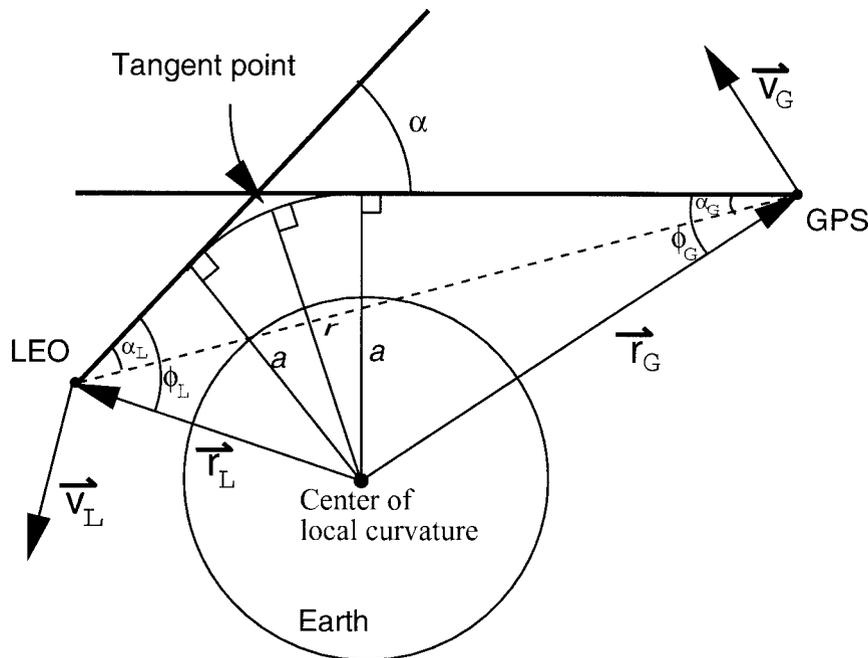E-mail: zou@met.fsu.edu

FIG. 1. Schematic representation of the LEO and GPS occultation geometry of GPS/MET, defining the occultation bending angle α, the impact parameter a, the satellites' radii $\mathbf{r}_G$ and $\mathbf{r}_L$, the satellite velocity vectors $\boldsymbol{v}_G$ and $\boldsymbol{v}_L$, and the radius to the ray periapsis tangent point r.

inversion (Fjeldbo et al. 1971; Kursinski et al. 2001). The refractivity is a function of electron density in the ionosphere and temperature, pressure, and water vapor in the neutral atmosphere. The two (L1 and L2) frequencies enable the ionospheric effects to be separated from the neutral atmosphere effects. Given the refractivity in the neutral atmosphere and using the hydrostatic equation, it is possible to calculate the temperature, pressure, and geopotential when water vapor's contribution is negligible above the lowest scale height (e.g., at temperatures below 250 K in the troposphere, i.e., above 5–7 km). In the low troposphere when water vapor has an appreciable effect on GPS occultation measurements, it is possible to derive temperature and water vapor if independent estimates of either temperature or water vapor are known.

Various strategies for assimilating radio occultation data are discussed by Eyre (1994) and Kuo et al. (2001). Briefly, it is possible to assimilate bending angles, refractivity, or derived temperature and water vapor profiles. Because the retrieval of the bending angle requires the fewest assumptions, Eyre (1994) and others suggest that the most accurate results will be obtained by assimilation of bending angles rather than refractivities, temperature, and water vapor. However, assimilation of bending angles requires either the use of a ray-tracing model or the forward Abel inversion to compute the bending angles from the model analysis first-guess fields using a variational procedure (Palmer et al. 2000; Zou et al. 1999, 2000). A 3D ray-tracing model is most accurate, but is computationally very expensive. Therefore, it is useful to investigate whether a computationally more efficient 2D ray-tracing model will give acceptable results.

The variational analysis of the atmospheric state requires the specification of the error characteristics of each type of observation. Zou et al. (1999) described a 2D ray-tracing model and its tangent linear and adjoint operators. These operators were linked to the National Centers for Environmental Prediction (NCEP) Spectral Statistical Interpolation analysis system to conduct the GPS/MET data assimilation experiment (Matsumura et al. 1999; Zou et al. 2000). However a crude estimate of the bending angle error variances was used in both studies. In this paper we develop a statistical estimate of the bending angle errors that arise through the assumption of spherical symmetry and a 2D ray-tracing model. We use the orbital parameters from 133 soundings obtained from the GPS/MET experiment and the NCEP analysis fields to compute the "true" bending angle profiles using an accurate 3D ray-tracing procedure. This technique does not require the spherical symmetry assumption. We then estimate the bending angles using the 3D ray-tracing model with the spherical symmetry assumption. This estimate, which we call the "pseudo–" bending angle, is analogous to obtaining the retrieved bending angles from the radio occultation technique. Finally, we obtain a third estimate of the bending angle using a fast 2D ray-tracing model rather than the 3D model. Comparison of these three estimates of bending angle yields a statistical estimate of the errors associated with the spherical symmetry assumption and the 2D forward ray-tracing model. We do not consider

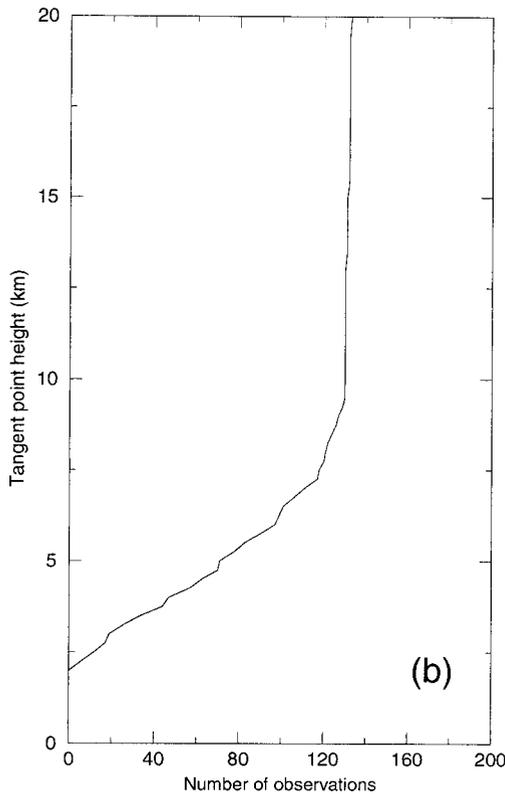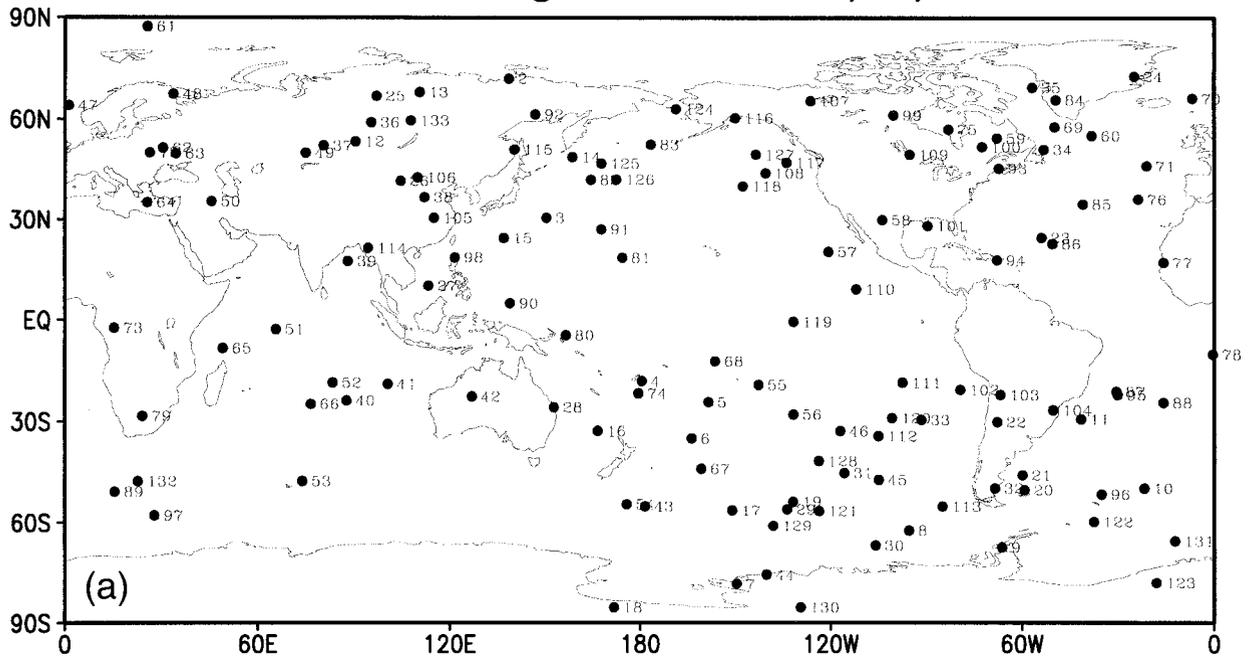## GPS sounding location for 10/11/95

FIG. 2. (a) The global coverage of all the GPS occultations received from the *MicroLab-1* satellite during a 24-h period centered at 1200 UTC 11 Oct 1995. Each occultation sounding is numbered in the order of its receiving time. (b) The total number of observations at each altitude.

other errors associated with the radio occultation technique; these are described and discussed by Lipa and Tyler (1979), Kursinski et al. (1997, 2001), Feng and Herman (1999), Palmer et al. (2000), and others.

The error characteristics of radio occultation data due to the assumption of spherical symmetry have been studied by Gavrik and Samoznaev (1985), Ahmad and Tyler (1999), and Healy (2001). Gavrik and Samoznaev
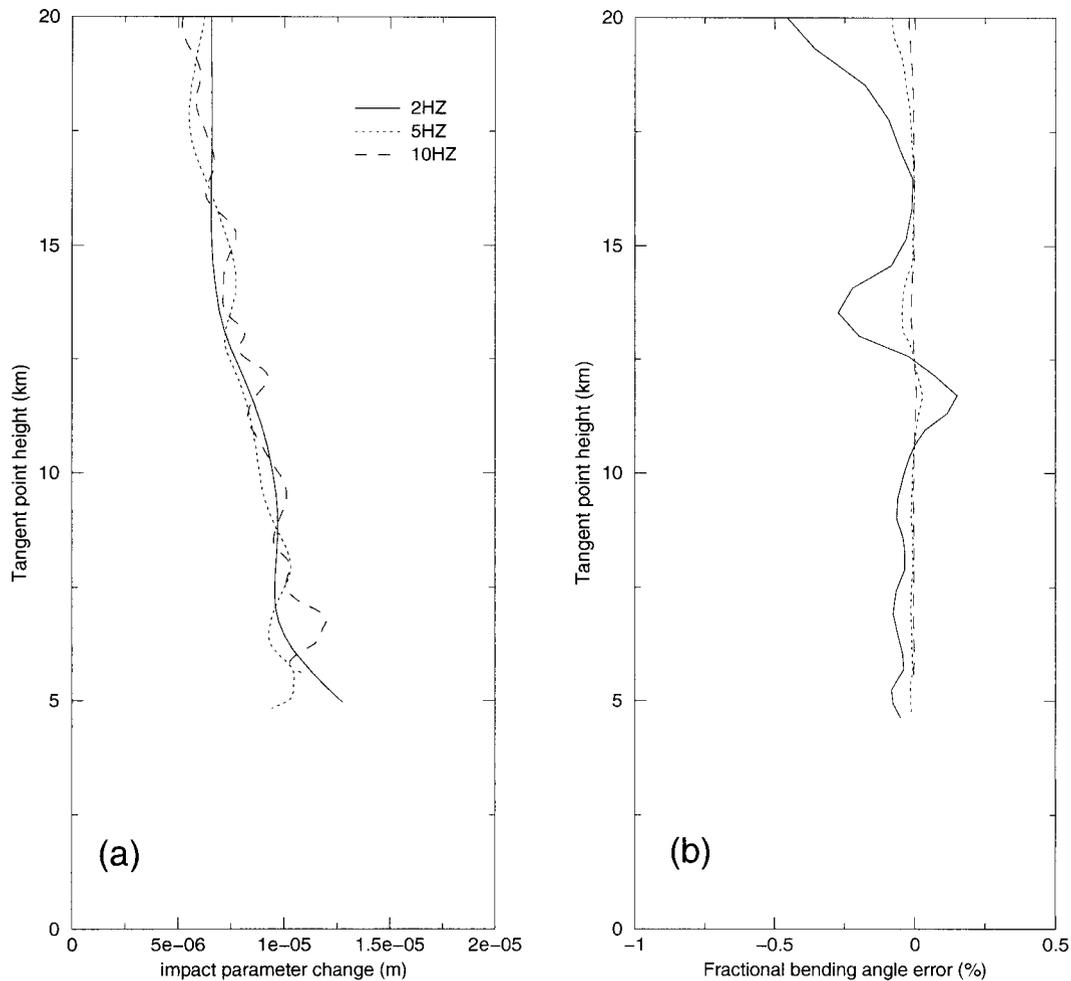
FIG. 3. (a) The maximum change of impact parameter along each ray (e.g., the difference between the maximum and minimum values of impact parameter along the ray path) in the 3D ray-tracing model in a spherically symmetric medium using 2-, 5-, and 10-Hz vertical resolutions. The earth is assumed spherical. A smooth vertically decaying refractivity profile, obtained by a horizontal average of the NCEP analysis of refractivity is used. Inputs for the 3D ray-tracing model are from the GPS/MET level-2 data for GPS-75. Experiments are carried for 2-, 5-, and 10-Hz vertical resolutions. (b) The corresponding fractional errors of bending angle.

(1985) analyzed errors in radio-occultation results for the ionosphere of Venus due to its asphericity. Ahmad and Tyler (1999) and Healy (2001) estimated errors in radio-occultation results for the troposphere of earth due to the spherical symmetry assumption. Errors caused by the across-track refractivity gradient in the troposphere of earth were studied by Ahmad and Tyler (1999). Their simulation results, using refractivity derived from a relatively coarse resolution forecast model (7.5° in latitude and 9.0° in longitude), indicated that the fractional error in the bending angle due to the spherical symmetry assumption is about 1% between 30 and 40 km, decreasing linearly away from this height range. The errors caused by the across-track refractivity gradient for the impact parameter were about 100 m in the lower troposphere, decreasing linearly with height. Healy (2001) used refractivity fields derived from a set of 12.3-km

6-h mesoscale forecasts for his study of the errors introduced by the spherical symmetry assumption. His results indicated that the errors caused by the across-track refractivity gradient could be as high as 0.08% for an individual bending angle profile and 60 m for the impact parameter. The errors caused by the along-track gradient were about 0.01% for the bending angle and 120 m for the impact parameter. However, the 54 randomly chosen forecasts are located at the same location in the United Kingdom. It is important to use a relatively large data sample that contains meteorological situations in Tropics as well as mid- and high latitudes to estimate the observation error covariances.

In section 2 we discuss the methodology for estimating the bending angle errors caused by the spherical symmetry assumption. The forward model used for the assimilation of the bending angles and its error estimate

are discussed in section 3. Section 4 contains the method used to estimate the mean errors and error covariances of the bending angle calculations. The results are discussed in section 5.

2. Brief description of variational data assimilation problems

Among many of the atmospheric data assimilation techniques, the variational data assimilation scheme, which employs the adjoint techniques, appears to be the most promising approach for the assimilation of indirect observations. The objective of variational data assimilation is to find an ''optimal'' model state that best fits various observations distributed within a certain space and time interval. More specifically, in variational data assimilation, one attempts to minimize a cost function

$$2J(\mathbf{x}) = (\mathbf{x} - \mathbf{x}_b)^{\mathrm{T}}\mathbf{B}^{-1}(\mathbf{x} - \mathbf{x}_b)$$
$$+ [\mathbf{d} - H(\mathbf{x})]^{\mathrm{T}}(\mathbf{O} + \mathbf{F})^{-1}[\mathbf{d} - H(\mathbf{x})], \quad (1)$$

where $\mathbf{x}$ is the analysis vector of the atmospheric state on the analysis/forecast grid, $\mathbf{x}_b$ is the forecast background vector, $\mathbf{d}$ is a vector of observations, $\mathbf{B}$ is the background error covariance matrix, $\mathbf{O}$ is the observation error covariance matrix, $\mathbf{F}$ is the forward model error covariance matrix, and H is the forward model (often called observation) operator, which calculates the observed quantities based on the model state $\mathbf{x}$.

The first term (the background term) in (1) measures the misfit between the model state and a known background field. The second term (the observation term) measures the distance between the model state and the observations. The observation term usually consists of several individual terms J_i^o corresponding to various types of observations.

The variational approach can directly assimilate any measurements as long as they can be expressed as a function of the basic forecast model state variable through a physical model and/or an interpolation procedure. A priori ''retrieval'' is not required. For example, the GPS occultation measurements of bending angles can be directly assimilated without a priori retrieval of temperature and moisture profiles. Because of various assumptions used, the a priori retrieval often introduces errors whose characteristics are difficult to derive. The ability to directly assimilate a rawer form of measurements and make global adjustments using all available observations are important features of the variational technique.

The ''optimal'' solution $\mathbf{x}^*$ of the atmospheric state is obtained by minimizing J based on the values of J and its gradient, which can be expressed as

$$\nabla J(\mathbf{x}) = \mathbf{B}^{-1}(\mathbf{x} - \mathbf{x}_b) + \mathbf{H}^{\mathrm{T}}(\mathbf{O} + \mathbf{F})^{-1}[\mathbf{d} - H(\mathbf{x})], \quad (2)$$

where $\mathbf{H}$ and $\mathbf{H}^{\mathrm{T}}$ are the tangent linear and adjoint operators of H, respectively.

Examining (1)–(2), the work required for adding a new type of observations into an existing variational data assimilation system includes (i) developing a proper forward observation operator (H) for the observed quantities, its corresponding tangent linear and adjoint operators ($\mathbf{H}$ and $\mathbf{H}^{\mathrm{T}}$), and (ii) estimating the observation and forward model error covariances ($\mathbf{O}$ and $\mathbf{F}$) of that specific observations.

Numerical and physical considerations for a 2D ray-tracing model H for GPS bending angle, along with its tangent linear and adjoint operator $\mathbf{H}$ and $\mathbf{H}^{\mathrm{T}}$, were described in Zou et al. (1999). This paper provides a method for estimating $\mathbf{O}$ and $\mathbf{F}$. This work is motivated by the following purposes: (i) to carry out bending angle assimilation experiments using a realistic nondiagonal observational error covariance matrix, (ii) to test methods of assimilating GPS refractivity with an accuracy of analysis close to that obtained by assimilating GPS bending angle, and (iii) to conduct a series of realistic observing system simulation experiments (OSSES) of GPS radio-occultation refractivity data assimilations that assess the potential impact of these new data on NWP. The 3D ray-tracing model that is used in the error estimate can be used to generate the GPS bending angle observations, followed by an operation of the Abel inversion to derive GPS refractivity observations. The use of the 3D ray-tracing model for creating simulated observations different from the assimilation model (the 2D ray-tracing model or the refractivity operator) prevents the OSSE results from being overly optimistic due to the use of observations that are not properly simulated.

3. Estimating observational errors due to the spherical symmetry assumption

Given the atmospheric refractivity field and the satellite positions and velocities, the bending angle and Doppler shift can be derived by solving the ray trajectory equation in 3D space. One such model is the 3D forward raytracing model described by Hoeg et al. (1995). The name of the ray-tracing model is ROSAP, which stands for Radio Occultation Simulation for Atmospheric Profiling. This model solves the ray equations in Cartesian coordinates, with a variable step size. The variable step size allows a faster ray integration for rays with no appreciable bending, such as those at high altitudes and/or far away from the tangent points (e.g., ≥ 500 km). The ray path that intersects both satellites is found using the ray-shooting method through an iterative procedure. The expected accuracy at the end point of the ray path, compared with the actual LEO satellite position, is within 1 mm.

We use this 3D ray-tracing model to estimate the true bending angle (denoted as α^{3D}) and bending angle errors due to the use of the spherical symmetry assumption and a 2D ray-tracing forward model. The satellite positions and velocities required by the 3D ray-tracing model are obtained from 133 observed GPS/MET ob-

servations. The Doppler shift obtained by the 3D ray-tracing model can also be processed with the standard GPS/MET data analysis technique (Rocken et al. 1997) to derive the pseudo–bending angle (denoted as $\alpha^{\text{3D-SYM}}$) under the spherical symmetry assumption. Having estimates of the bending angles with and without the spherical symmetry assumption, we examine the difference between $\alpha^{\text{3D-SYM}}$ and α^{3D}. However, this is not as straightforward as one might expect. The horizontal gradients of atmospheric refractivity distribution cause the impact parameter to vary when a radio signal travels from a GPS transmitter to a LEO receiver. The 3D bending angle does not correspond to a single-value impact parameter.

As an approximation, α^{3D} is first taken as a function of the impact parameter at the tangent point (a_t), $\alpha^{\text{3D}} = \alpha^{\text{3D}}(a_t)$, where a_t is defined as the value of the impact parameter at the point on the simulated ray that is closest to the earth's surface. This vertical profile of the bending angle in terms of the impact parameter at the tangent point is then transformed into a vertical profile of the bending angle in terms of the tangent point height [$\alpha^{\text{3D}}(z)$] by a simple variable transform $a_t = n(z + r_{\text{loc}})$, where n is the refractive index taken from the NCEP model at the tangent point and r_{loc} is the radius of local curvature of the actual earth of the observed occultation. The earth is assumed spherical with a radius of r_{loc} for the simulations of all the rays of each occultation. For different occultations, r_{loc} is different. The function $\alpha^{\text{3D-SYM}}$ ($\alpha^{\text{3D-SYM}}$) is converted to a function of height $\alpha^{\text{3D-SYM}}(z)$ through the same form of the variable transform $\alpha^{\text{3D-SYM}} = n(z + r_{\text{loc}})$. The two bending angle vertical profiles can finally be differenced to obtain an error vector:

$$\boldsymbol{\epsilon}^{\text{3D}}_{\text{GPS}}(z) = \alpha^{\text{3D-SYM}}(z) - \boldsymbol{\alpha}^{\text{3D}}(z). \tag{3}$$

The mean and covariance matrix of $\boldsymbol{\epsilon}^{\text{3D}}_{\text{GPS}}$ provide an estimate of the mean error and error covariances due to the departures from spherical symmetry in the model atmosphere. The simulated bending angle vertical profiles are interpolated from a 10-Hz resolution (see section 6a for more discussions on resolution) to a standard vertical resolution of 0.25 km below 10 km, 0.5 km between 10 and 20 km, and 1 km above 20 km for the required statistical calculations.

4. Estimating the forward model errors

The 3D ray-tracing model is computationally expensive; hence, a cheaper alternative that may produce acceptable GPS/MET data assimilation results is to use the 2D ray-tracing model. For example, the 2D model simulates a single occultation with 380 rays in 2.9 CPU seconds on a Cray J90, while the 3D raytracing model simulates the same occultation on the same computer in 18.7 CPU seconds. It is necessary to estimate the errors that result from the use of this simplified forward model if it is used for bending angle assimilation. Com-

pared with the 3D ray-tracing model, the key feature of this 2D model (Zou et al. 1999) is that the ray-tracing is carried out in a 2D occultation plane, which is defined as a plane that contains the tangent point of the observed GPS occultation, the GPS satellite, and the center of the local curvature at the tangent point. The gradient of refractivity perpendicular to the 2D occultation plane is neglected. In this study, all the input information for the 2D ray-tracing model is obtained from the 3D ray-tracing model, instead of those from GPS/MET observational retrievals in the case of bending angle data assimilation. The ray equations are then integrated, starting from the GPS satellite position, with either a fourth-order Runge–Kutta method or the alternating direction implicit method (Yanenko 1971) with a fixed step size of 1 km. The ray tracing continues until the ray goes out of the atmosphere, which is assumed to be at a distance of more than 100 km from the ray to the earth's surface. The position and the tangent direction of the ray at the ending point of the simulated ray are taken as those at the LEO satellite. Finally, the bending angle of the ray is calculated by the angle between the two tangent directions at the starting and ending points of the ray. Numerical details of the scheme are summarized in Zou et al. (1999).

Applying the same procedure as was done for the 3D bending angles, a vertical profile of the bending angle simulated by the 2D raytracing forward model can be obtained and is denoted as $\alpha^{\text{2D}}(z)$. The forward model errors can then be estimated by examining the mean, the variances, and the correlations of the following vector:

$$\boldsymbol{\epsilon}^{\text{2D}}_{\text{F}}(z) = \alpha^{\text{2D}}(z) - \boldsymbol{\alpha}^{\text{3D}}(z). \tag{4}$$

If $\alpha^{\text{3D-SYM}}$, instead of $\boldsymbol{\alpha}^{\text{3D}}$, is used in (4), the difference would be related to both the spherical symmetry errors and the 2D forward model errors.

5. A description of ray-tracing experiments and error analysis for GPS bending angle

Both the 2D and 3D ray-tracing models require input values of atmospheric refractivity N, and the vertical and horizontal gradients of N along the ray. The NCEP triangle 28-layer 62-wave global analyses (written as T62L28) and the Committee on Space Research (COSPAR) International Reference Atmosphere (CIRA) data[1] are combined to produce the refractivity fields from the earth's surface to a height of 120 km above the surface for both models. Refractivities are calculated from the NCEP analysis of temperature, specific humidity, and surface pressure with a horizontal resolution of approximately 1.875° (0.0327 rad). The vertical coordinate of the model is $\sigma = 1 - p/p_*$, defined by Phillips (1959)

---

[1] The CIRA data (see COSPAR International Reference Atmosphere special issue of *Advances in Space Research,* 1990; Vol. 10, No. 12) are used above the highest level of the NCEP model.

and Sela (1980), where p is the pressure and p_* is the surface pressure. The 28 vertical layers extend from the surface (where $\sigma = 0$) to the NCEP model top at about 35 km (where $\sigma = 1$). The CIRA atmospheric model covers the range from 35 to 120 km. The smooth transition from the NCEP fields to CIRA data is made for both the refractive index and the gradient of refractive index (see appendix 3 in Zou et al. 1999).

In the 2D ray-tracing model, the vertical gradient of the refractivity is calculated numerically using finite differences on the NCEP and CIRA model grids. Then the derivative is interpolated to Cartesian coordinates during the ray integration. In the 3D model, however, the horizontal and vertical derivatives of the refractivity are calculated in Cartesian coordinates during the ray integration. The satellite coordinates and velocities required by the 3D ray-tracing model are obtained from the GPS/MET observations. The normal direction of the occultation plane and the tangent point position required by the 2D ray-tracing model are obtained from the 3D ray-tracing results.

The bending angle profiles are derived from the NCEP global analysis at 1200 UTC 11 October 1995. We had 133 observed GPS/MET occultations for the 24-h period centered at this time. The geographical distribution of these soundings is shown in Fig. 2a. These are the data within the prime period 3 of GPS/MET when antispoofing (e.g., a GPS encryption device) was turned off. Of the 133 soundings, however, fewer than 15 soundings reached below 2.5 km (Fig. 2b).[2] Therefore, results below 2.5 km are omitted in any statistics.

In the following, we will examine the mean fractional errors, the variances, and the vertical correlations described by the vectors $\boldsymbol{\epsilon}_{GPS}^{3D}$ and $\boldsymbol{\epsilon}_{F}^{2D}$, calculated over these soundings. The covariance matrices of $\boldsymbol{\epsilon}_{GPS}^{3D}$ and $\boldsymbol{\epsilon}_{F}^{2D}$ will be denoted as

$$\mathbf{O}^{GPS} = \overline{(\boldsymbol{\epsilon}_{GPS}^{3D} - \overline{\boldsymbol{\epsilon}}_{GPS}^{3D})(\boldsymbol{\epsilon}_{GPS}^{3D} - \overline{\boldsymbol{\epsilon}}_{GPS}^{3D})^{T}} \qquad (5)$$

$$\mathbf{F}^{2D} = \overline{(\boldsymbol{\epsilon}_{F}^{2D} - \overline{\boldsymbol{\epsilon}}_{F}^{2D})(\boldsymbol{\epsilon}_{F}^{2D} - \overline{\boldsymbol{\epsilon}}_{F}^{2D})^{T}}, \qquad (6)$$

where the overbar is an average over all the soundings involved in estimation. The matrix $\mathbf{O}^{GPS}$ describes the error characteristics due to the spherical symmetry assumption. If the pseudo–bending angles and impact parameters, which are given by GPS observations, are simulated in the forward model (as was attempted in the 2D ray-tracing model described here), $\mathbf{O}^{GPS}$ is not required in forming the inverse weighting matrix for bending angle data assimilation. The inverse weighting matrix will consist of only $\mathbf{F}^{2D}$ and other parts of the observational errors such as measurement errors, calibration errors, and representativeness errors.

***

[2] The reasons for the small number of soundings reaching the lowest 2 km of the troposphere are described by Rocken et al. (2001, p. 45). COSMIC expects to track 90% of all occultations into the lowest 1 km of the atmosphere.
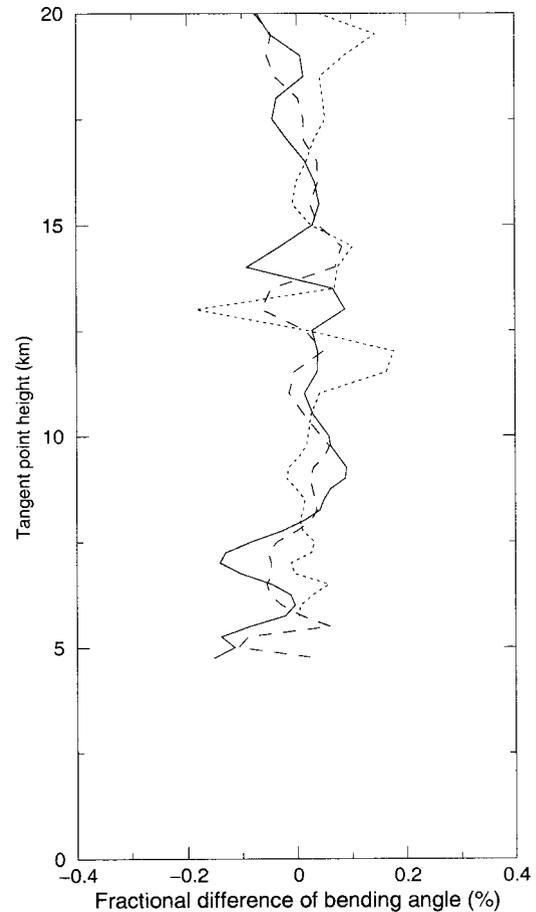

FIG. 4. The values of $(\alpha^{2D} - \alpha^{3D})/\alpha^{3D}$ as functions of height for a spherically symmetric medium using orbital parameters from the three GPS/MET soundings: GPS-48 (solid), GPS-75 (dashed), and GPS-79 (dotted).

6. Numerical results

a. Vertical sampling for the bending angle simulations

The phase delays are converted into bending angle and ray impact parameter using the finite-difference method in the 3D ray-tracing model. The accuracy of the calculated $\alpha^{3D\text{-}SYM}$ is therefore found to be sensitive to the vertical resolution of the simulated rays for each occultation. We have tested the 3D symmetric bending angle simulation at 2-, 5-, and 10-Hz intervals, resulting in about 120, 300, and 600 rays for each occultation, respectively. The accuracy of the ray tracer and the sufficiency of the vertical resolution can be tested in a spherically symmetric medium (assuming the earth is spherical and the horizontal gradient of the refractive index is zero) in two ways. First, the impact parameter should be constant along the ray path. Second, the fractional error of the bending angle due to the spherical symmetry assumption should be zero. For a smooth vertically decaying refractivity profile, obtained from a hor-
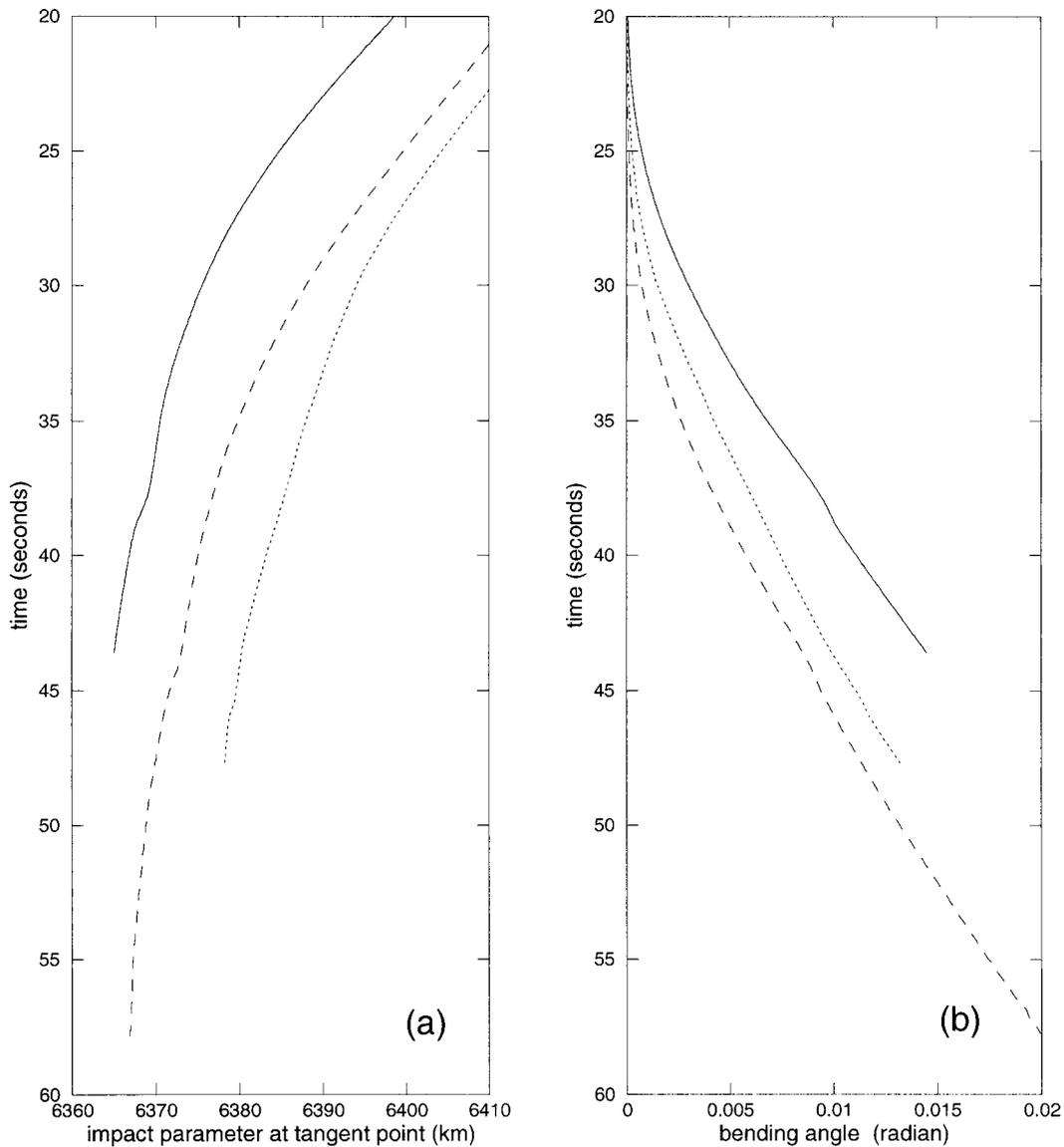
FIG. 5. (a) The impact parameter at the tangent point and (b) the bending angle $\alpha^{\text{3D-SYM}}$ as functions of time for the three selected GPS/MET soundings: GPS-48 (solid), GPS-75 (dashed), and GPS-79 (dotted).

izontal average of the NCEP analysis of the refractivity field, the impact parameter varies by less than 1.25×10^{-5} m along the ray for the 2-, 5-, and 10-Hz vertical resolutions (Fig. 3a). The fractional error of $\alpha^{\text{3D-SYM}}$ increases from around 0.1% in the troposphere to 0.5% at 20 km when a coarse vertical resolution 2 Hz is used for the bending angle simulation (Fig. 3b, solid line). Such an error is much larger than a theoretical value of the error caused by the impact parameter change. If the impact parameter is off by 1.25×10^{-5} m, the calculated bending angle will be in error by about 1.6×10^{-7}%, assuming the bending angle falls exponentially with the impact parameter in an atmosphere with an 8-km scale height. Increasing the vertical resolution to 5 (dotted line) and 10 Hz (dashed line) reduces the bending angle

fractional errors significantly. The errors at all heights are less than 0.1% and 0.025% for the 5-, and 10-Hz resolution, respectively. However, experiments performed in which the vertical resolution is further increased showed only small improvements in the accuracy of the 3D symmetric model, while the computational cost increased tremendously. We have therefore used 10-Hz vertical resolution for all the 2D and 3D bending angle simulations.

The sampling problem discussed above might be mitigated with the use of a better numerical differentiation algorithm, such as the spectral differentiator (Anderssen and Bloomfield 1974a,b). The final conclusion on the vertical sampling rate depends also on how the typical stochastic errors for the observed phase delays propa-
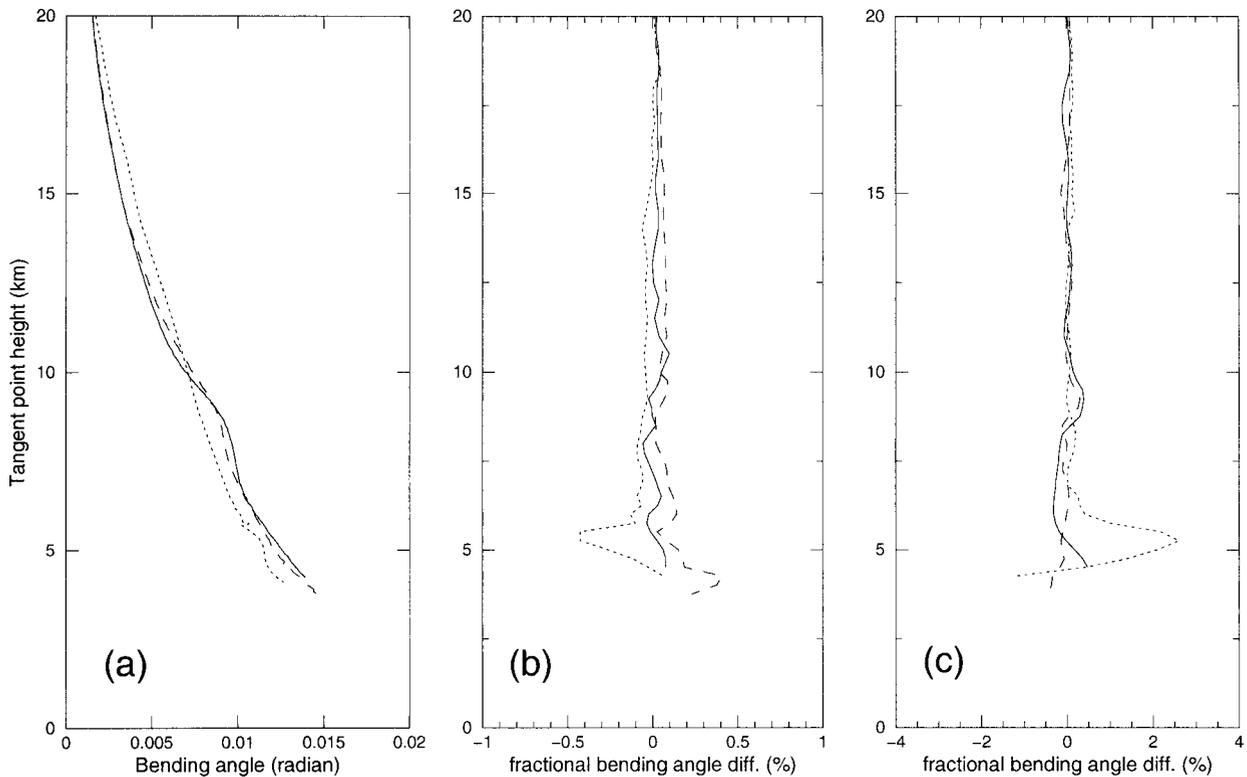
FIG. 6. The values of (a) $\alpha^{3D\text{-}SYM}$, (b) $(\alpha^{3D\text{-}SYM} - \alpha^{3D})/\alpha^{3D}$, and (c) $(\alpha^{2D} - \alpha^{3D})/\alpha^{3D}$ as functions of height for the three GPS/MET soundings: GPS-48 (solid), GPS-75 (dashed), and GPS-79 (dotted).

gate to the errors in the retrieved bending angle, which is not included in this study.

b. Simulation of individual bending angle profiles and their errors

Departures from spherical symmetry come from not only the horizontal gradients of the refractive index, but also the ellipsoidal shape of the earth. The later kind of errors can be removed through an oblateness correction of the simulated impact parameters (Syndergaard 1998). In order to concentrate on the errors caused by horizontal gradients in the atmosphere, the earth is assumed spherical in all of the following 2D and 3D simulations.

Before assessing the 2D forward model errors caused by across-track gradients of refractivity, a control experiment is carried out to evaluate the intrinsic forward model errors due to the different numerical schemes used in the 2D and 3D models. Figure 4 shows the values of $(\alpha^{2D} - \alpha^{3D})/\alpha^{3D}$ as functions of height for a spherically symmetric medium using orbital parameters from the three GPS/MET soundings: GPS-48 (solid), GPS-75 (dashed), and GPS-79 (dotted). The 2D model errors of bending angle due to numerics are less than 0.2%.

Figure 5 shows the behavior of the ray impact parameter at the tangent point (panel a) and the bending angle (panel b) as functions of time for the three oc-

cultations corresponding to GPS-48, GPS-75, and GPS-79 (see Fig. 2a for their locations) using the 3D ray-tracing model with the spherical symmetry assumption and the NCEP analysis at 1200 UTC 11 October 1995. These three GPS/MET soundings occurred at (68°N, 40°E; 0732 UTC), (57°N, 83°W; 1222 UTC), and (28°S, 24°E; 1280 UTC) 11 October 1995, respectively. The lowest height that each sounding reaches is determined either by the lowest ray that does not intercept the earth or the real soundings limit that was due to the loss of tracking in the lowest kilometers. Figure 5a provides an idea of how the sampling rate discussed in section 6a is related to the vertical sampling of the atmosphere. The lines in Fig. 5a indicate that a constant sampling rate (e.g., 10 Hz or equivalently 0.1 s) produces higher vertical resolution in the low levels than the upper levels. The simulated bending angle, as well as the fractional errors of the 3D and 2D model simulations as a function of height corresponding to these three occultations are shown in Fig. 6. The monotonic decreasing behavior of bending angle with height observed in Fig. 5b is not seen in Fig. 6a due to the involvement of the refractive index n in the conversion from the impact parameter to the height ($z = a/n - r_{loc}$). Differences between the ''true'' bending angle and the pseudo–bending angle derived from the 3D ray-tracing model (i.e., $\alpha^{3D\text{-}SYM} - \alpha^{3D}$) and those from the 2D ray-tracing model (i.e., $\alpha^{2D} - \alpha^{3D}$) are shown in Figs. 6b and 6c, respec-

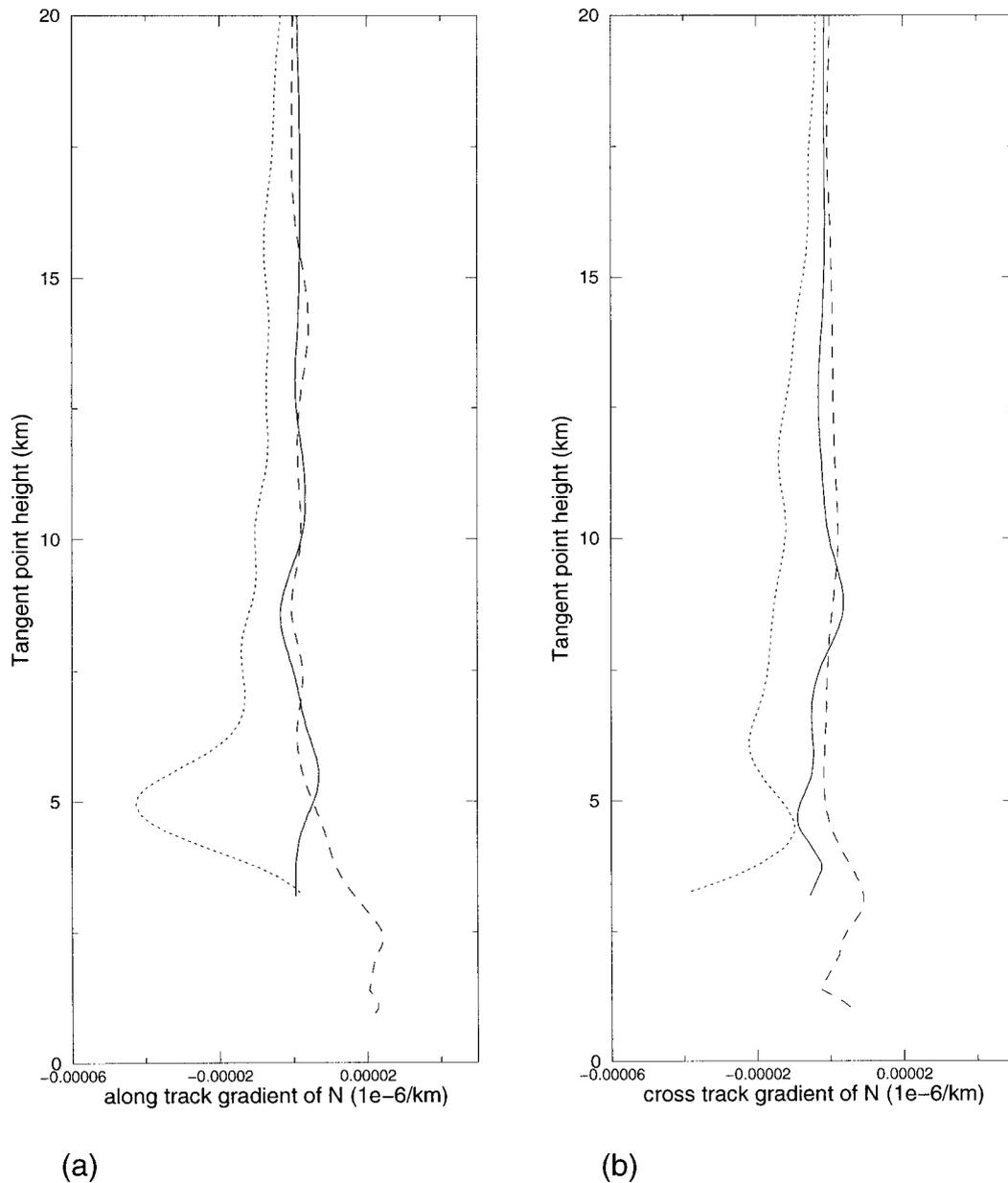(a)   (b)

FIG. 7. Vertical profiles of (a) along-track and (b) across-track gradients of refractivity for the three GPS/MET soundings: GPS-48 (solid), GPS-75 (dashed), and GPS-79 (dotted).

tively. The magnitude of the difference between the 2D and 3D simulation varies with the sounding location. The fractional errors of the bending angle due to the spherical symmetry assumption can be as large as 0.5%, and those due to the forward model errors can be as large as 2.5% (Figs. 6b and 6c). Both types of errors approach zero at high altitudes. The extremum at 5 km observed for both differences $\alpha^{3D\text{-}SYM} - \alpha^{3D}$ and $\alpha^{2D} - \alpha^{3D}$ for the tropical profile (GPS-79) is caused by the large horizontal gradient of refractivity at this height (see Fig. 7a). The difference between the two fractional errors (Figs. 6b and 6c) reflects mainly the effect of the

across-track horizontal gradients (Fig. 7b). It is worth mentioning that the errors due to the numerical differences between the 3D and 2D ray-tracing models (Fig. 4) are more than one order of magnitude smaller that those due to the effect of horizontal gradients (Fig. 6c).

The impact parameters for these three GPS soundings vary along the ray path. As an example, the variations of the impact parameter along the ray path at 8 km (the tangent point height) in the 3D simulation are shown in Fig. 8. Most variations in the impact parameter begin at 400 km from the tangent point and are small in magnitude (less than 12 m).
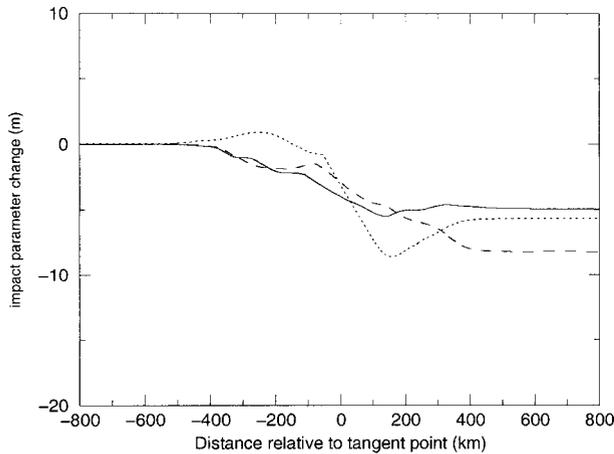
FIG. 8. The variation of impact parameter as a function of the distance from all the grid points in a ray integration to the tangent point of the ray at 8-km height: GPS-48 (solid line), GPS-75 (dashed line), and GPS-79 (dotted line). The 3D ray-tracing model is used.

The vertical variations of the maximum change of the impact parameter along each ray (e.g., the difference between the maximum and minimum values of impact parameter along the ray path) for these three soundings are shown in Fig. 9. They provide an overall measure on the effect of the spherical symmetry assumption at all heights. The impact parameter along each ray caused by the horizontal gradient of refractivity can vary up to about 45 m below 5 km in both the 3D and 2D models (Figs. 9a,b). A 1-km resolution or higher for ray integration is necessary for the 2D model results to compare well with those of the 3D model. At 20 km above the surface, the impact parameter variation becomes very small ($\leq$5 m) in both ray-tracing models. The vertical oscillations in the two figures for the same sounding (Figs. 9a, 9b) are similar, which is to be expected since the 2D and the 3D simulations experience much the same environment.

c. Simulation of statistical errors

Direct incorporation of GPS bending angle measurements requires the removal of bias errors of observations, as well as the knowledge of the statistical information of the observation error covariances. We, therefore, calculate the fractional errors, the rms errors, and the vertical error correlations of bending angle using the NCEP analysis fields and the orbital parameters from the 133 occultations obtained from the GPS/MET experiment during the 24-h period centered at 1200 UTC 11 October 1995. The average fractional errors due to the spherical symmetry assumption (Fig. 10, solid line) are less than 0.10% in the troposphere and reduce to 0.02% at about 20 km. The 2D ray-tracing forward model errors (Fig. 10, dashed line) have a maximum value of about 0.15% in lower troposphere and reduce to 0.03% above 15 km. The 0.15% fractional error cor-
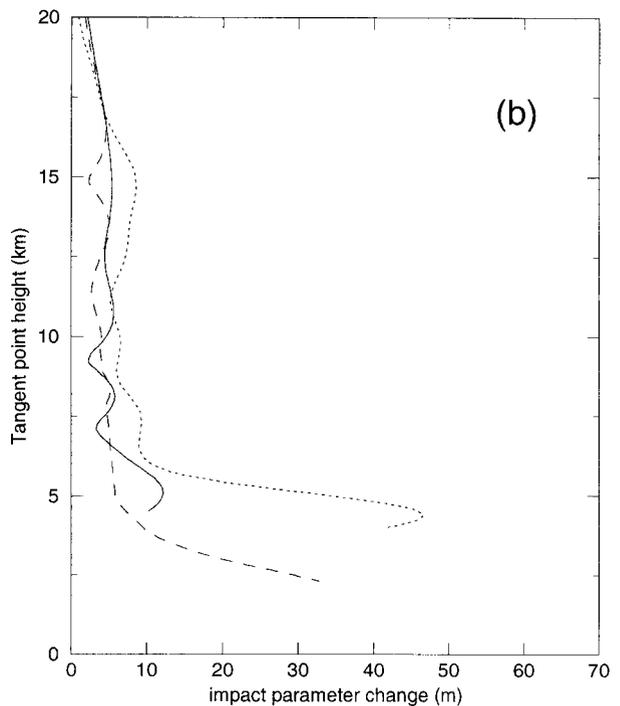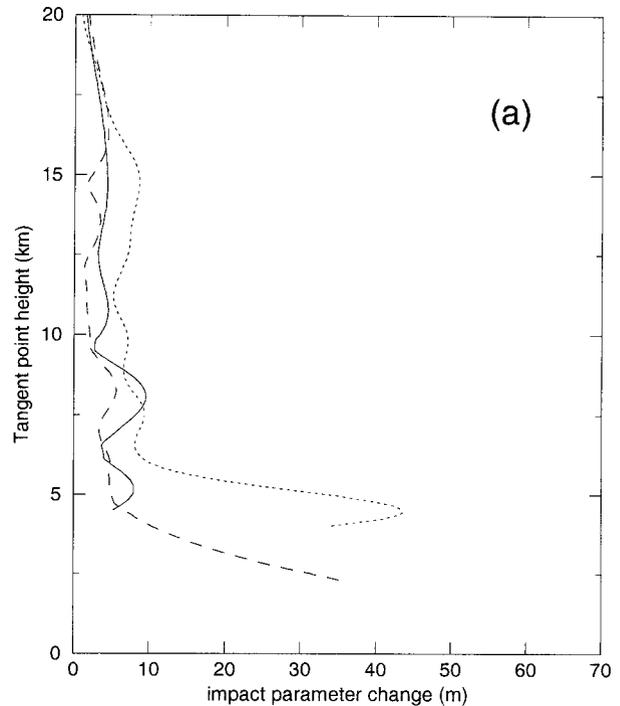

FIG. 9. Vertical profiles of the maximum change of impact parameter along each ray in the (a) 3D and (b) 2D ray-tracing models: GPS-48 (solid), GPS-75 (dashed), and GPS-79 (dotted).
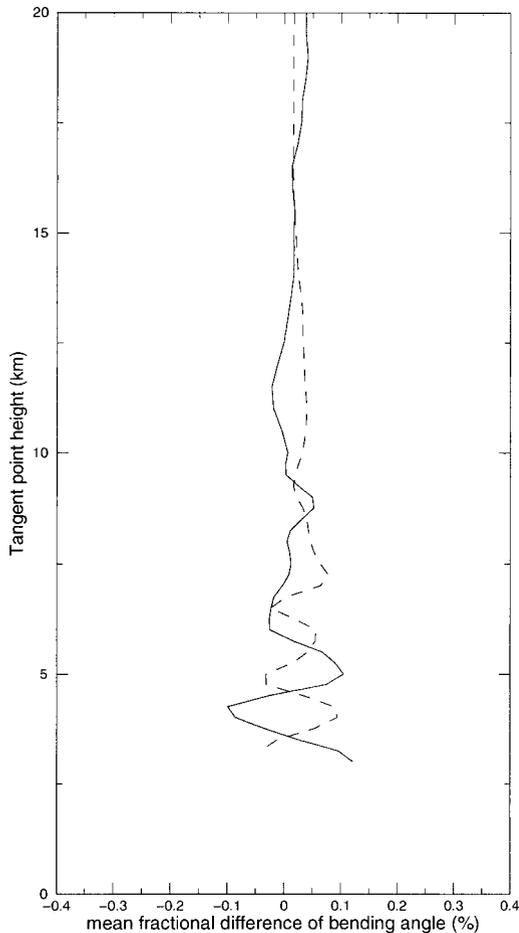
FIG. 10. The mean fractional errors of bending angle due to the spherical symmetry assumption (i.e., $\overline{(\alpha^{3D\text{-}SYM} - \alpha^{3D})/\alpha^{3D}}$) (solid line) and the 2D forward model errors (i.e., $\overline{(\alpha^{2D} - \alpha^{3D})/\alpha^{3D}}$) (dashed line).

responds to a bending angle error of 2.3×10^{-5} rad, given the mean value of the bending angle as 1.6×10^{-2} rad. The magnitudes of the average fractional errors of the forward model are slightly larger than the errors caused by the spherical symmetry assumption.

Figure 11 shows the vertical distribution of the rms of the error vectors $\boldsymbol{\epsilon}_{GPS}^{3D}$ (Fig. 11a, solid line) and $\boldsymbol{\epsilon}_{F}^{2D}$ (Fig. 11a, dashed line), the average differences between the maximum and minimum impact parameter values of each ray in both models (Fig. 11b), and the vertical correlations of the error vector $\boldsymbol{\epsilon}_{GPS}^{3D}$ and $\boldsymbol{\epsilon}_{F}^{2D}$ (Figs. 11c and 11d). The rms errors, and therefore the variances, decrease rapidly with height. Furthermore fluctuations in the rms errors are observed in the troposphere below 7 km. The 2D forward model errors (dashed line) are slightly larger than the errors caused by the spherical symmetry assumption (solid line). In the lower troposphere (2.5–5 km) the impact parameter varies, on average, by less than 20 m in both the 3D and 2D models. At higher altitudes, the changes in the impact parameter become smaller.

The vertical correlations of the bending angle errors due to the spherical symmetry assumption (Fig. 11c) are relatively sharp and decrease rapidly in the vertical between 6 and 8 km and become broader elsewhere. The vertical correlations of the 2D forward model errors (Fig. 11d) show a nearly diagonal structure below 15 km. Errors are only strongly correlated with levels that are less than 2 km away.

7. Summary and future work

In this study, a 3D ray-tracing model is used to study errors attributable to the spherical symmetry assumption that is used to derive bending angles from radio-occultation measurements of Doppler shift, and the forward model errors of a 2D ray-tracing model that is intended for use in bending angle data assimilation. The NCEP global model at T62L28 resolution is assumed to represent the real atmosphere and used for error estimations. The following are the main findings.

- The mean fractional errors of the bending angle due to the spherical symmetry assumption are less than 0.15%. The estimated errors due to the spherical symmetry assumption could be larger than those calculated here if the horizontal resolution of the model refractivity field is increased, or if the real atmosphere contains greater horizontal inhomogeneity than the model.
- The variation in impact parameter due to horizontal gradients in the atmosphere is only a few tens of meters along a ray in the lower troposphere, decreases with height, and reduces to almost zero at 20 km.
- The mean fractional errors and the rms errors associated with the 2D ray-tracing forward model are similar in magnitude to the errors caused by the spherical symmetry assumption. The forward model errors may be further reduced, for example, by incorporating the calculation of bending angle through Doppler shift into the 2D ray-tracing model so that the errors due to the spherical symmetry assumption will not be part of the forward model errors.
- The vertical correlations in the errors caused by the spherical symmetry assumption are strong within a ±2 km layer in the troposphere. They become broader above 9–10 km. The forward model error correlations are similar to those due to the spherical symmetry assumption except a sharper correlation is observed near 9 km.

These estimates of the error covariances in the retrieved bending angles due to the assumption of spherical symmetry and the use of a 2D rather than a 3D ray-tracing model can be used in 3DVAR or 4DVAR assimilation of bending angles in NWP models. The results indicate that these two sources of error in computing the bending angle are large compared to other sources of bending angle error (Kursinski et al. 1997, 2001). The results also indicate that we may use the
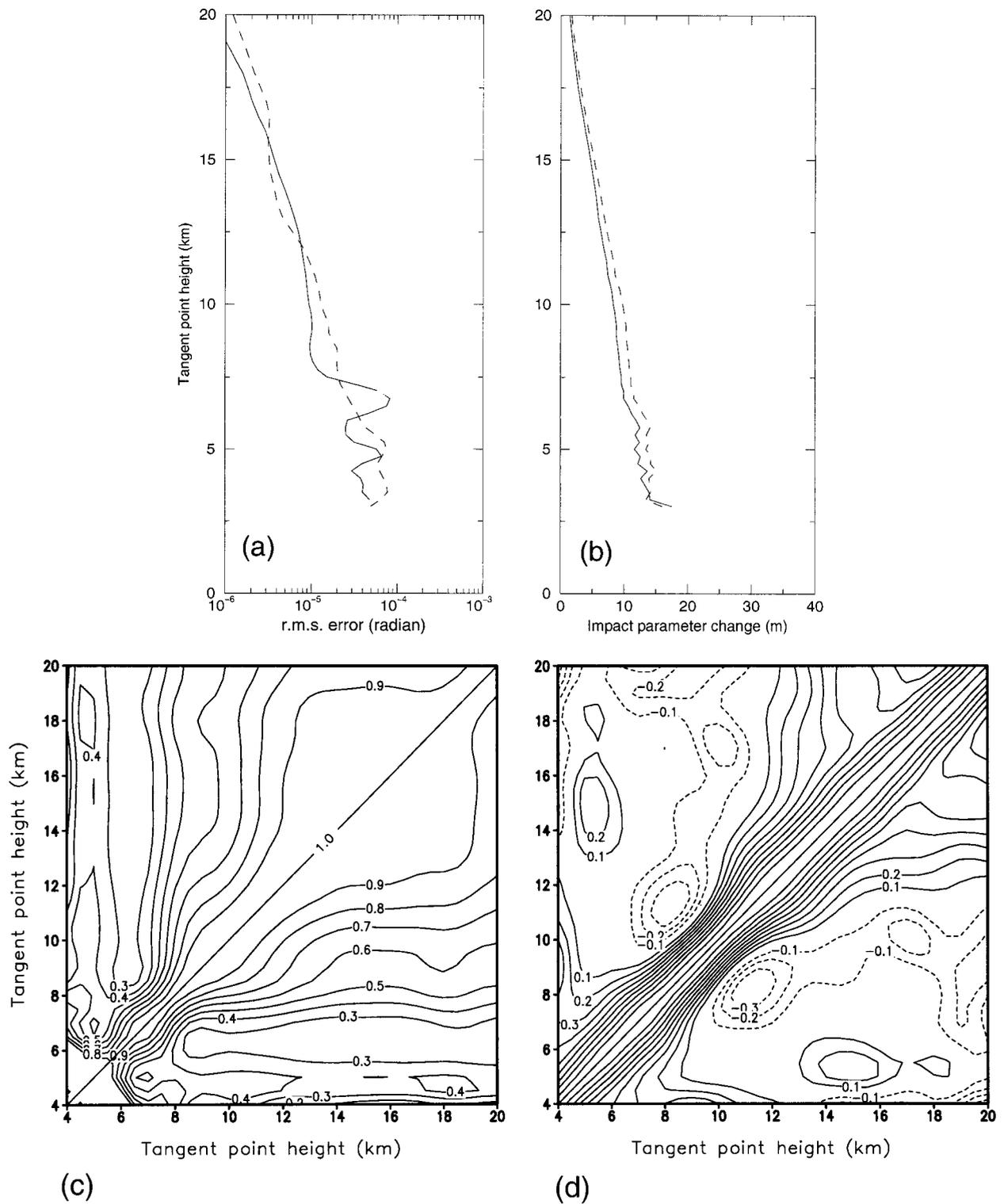
Fig. 11. (a) The rms of ϵ_{GPS}^{3D} (solid line) and ϵ_F^{2D} (dashed line), (b) the averaged maximum changes of impact parameter along each ray in the 3D model (solid line) and the 2D model (dashed line). The vertical correlations of the error vectors of ϵ_{GPS}^{3D} and ϵ_F^{2D} are shown in (c) and (d), respectively. The correlation patterns are symmetric about the diagonal given by the 1.0 correlation.

computationally more efficient 2D ray-tracing model rather than the more expensive 3D model in the assimilation of bending angles in NWP models. Results obtained from this work will be applied to future studies on the GPS bending angle assimilation.

REFERENCES

Ahmad, B., and G. L. Tyler, 1999: Systematic errors in atmospheric profiles obtained from Abelian inversion of radio occultation data: Effects of large-scale horizontal gradients. *J. Geophys. Res.,* **104,** 3971–3992.

Anderssen, R. S., and P. Bloomfield, 1974a: A time series approach to numerical differentiation. *Technometrics,* **16,** 69–75.

——, and ——, 1974b: Numerical procedures for non-exact data. *Numer. Math.,* **22,** 157–182.

Eshleman, V. R., 1973: The radio occultation method for the study of planetary atmospheres. *Planet. Space Sci.,* **21,** 1521–1531.

Eyre, J. R., 1994: Assimilation of radio occultation measurements into a numerical weather prediction system. ECMWF Tech. Memo., 199, 34 pp.

Feng, D. D., and B. M. Herman, 1999: Remotely sensing the earth's atmosphere using the Global Positioning System—The GPS/MET data analysis. *J. Atmos. Oceanic Technol.,* **16,** 989–1002.

Fjeldbo, G., G. A. Kliore, and V. R. Eshleman, 1971: The neutral atmosphere of Venus as studied with the Mariner V radio occultation experiments. *Astron. J.,* **76,** 123–140.

Gavrik, A. L., and L. N. Samoznaev, 1985: Analysis of errors in radio-occultation results for the daytime ionosphere of Venus due to its asphericity. *Kosm. Issled.,* **23,** 148–157.

Healy, S. B., 2001: Radio occultation bending angle and impact parameter errors caused by horizontal refractive index gradients in the troposphere: A simulation study. *J. Geophys. Res.,* in press.

Hoeg, P., A. Hauchecorne, G. Kirchengast, S. Syndergaard, B. Belloul, R. Leitinger, and W. Rothleitner, 1995: Derivation of the atmospheric properties using radio occultation technique. Danish Meteorological Institute Scientific Rep. 95-4, 208 pp.

Kuo, Y.-H., S. Sokolovskiy, R. Anthes, and F. Vandenberghe, 2001: Assimilation of GPS radio occultation data for numerical weather prediction. *Applications of Constellation Observing System for Meteorology, Ionosphere and Climate,* L.-C. Lee, C. Rocken, and R. Kurinski, Eds., Springer, 157–186.

Kursinski, E. R., and Coauthors, 1996: Initial results of radio occultation observations of Earth's atmosphere using the global positioning system. *Science,* **271,** 1107–1110.

——, G. A. Hajj, J. T. Schofield, R. P. Linfield, and K. R. Hardy, 1997: Observing Earth's atmosphere with radio occultation measurements using the Global Positioning System. *J. Geophys. Res.,* **102,** 23 429–23 465.

——, G. A. Hajj, S. Leroy, and B. Herman, 2001: The GPS radio occultation technique. *Applications of Constellation Observing System for Meteorology, Ionosphere and Climate,* L.-C. Lee, C. Rocken, and R. Kurinski, Eds., Springer, 53–114.

Lee, L.-C., C. Rocken, and R. Kursinski, Eds., 2001: *Applications of Constellation Observing System for Meteorology, Ionosphere and Climate.* Springer, 384 pp.

Lipa, B., and G. L. Tyler, 1979: Statistical and computational uncertainties in atmospheric profiles from radio occultation: Mariner 10 at Venus. *Icarus,* **39,** 192–208.

Lorenc, A., 1986: Analysis methods for numerical weather prediction. *Quart. J. Roy. Meteor. Soc.,* **112,** 1177–1194.

Matsumura, T., J. C. Derber, J. G. Yoe, F. Vandenberghe, and X. Zou, 1999: The inclusion of GPS limb sounding data into NCEP's global data assimilation system. NWS Office Note 426, NOAA/NCEP/NWS, 26 pp.

Palmer, P. I., J. J. Barnett, J. R. Eyre, and S. B. Healy, 2000: A nonlinear optimal estimation inverse method for radio occultation measurements of temperature, humidity and surface pressure. *J. Geophys. Res.,* **105,** 17 513–17 526.

Phillips, N. A., 1959: Numerical integration of the primitive equation on the hemisphere. *Mon. Wea. Rev.,* **87,** 333–345.

Rocken, C., and Coauthors, 1997: Analysis and validation of GPS/MET data in the neutral atmosphere. *J. Geophys. Res.,* **102,** 29 849–29 866.

——, Y.-H. Kuo, W. S. Schreiner, D. Hunt, S. Sokolovskiy, and C. McCormik, 2001: COSMIC system description. *Applications of Constellation Observing System for Meteorology, Ionosphere and Climate,* L.-C. Lee, C. Rocken, and R. Kurinski, Eds., Springer, 21–52.

Sela, J. G., 1980: Spectral modeling at the National Meteorological Center. *Mon. Wea. Rev.,* **108,** 1279–1292.

Syndergaard, S., 1998: Modeling the impact of the earth's oblateness on the retrieval of temperature and pressure profiles from limb sounding. *J. Atmos. Solar–Terr. Phys.,* **60,** 171–180.

Yanenko, N. N., 1971: *The Method of Fractional Steps.* Springer, 160 pp. Translated by M. Holt.

Ware, R., and Coauthors, 1996: GPS sounding of the atmosphere from low earth orbit: Preliminary results. *Bull. Amer. Meteor. Soc.,* **77,** 19–40.

Zou, X., and Coauthors, 1999: A raytracing operator and its adjoint for the use of GPS/MET refraction angle measurements. *J. Geophys. Res.,* **104,** 22 301–22 318.

——, B. Wang, H. Liu, R. A. Anthes, T. Matsumura, and Y.-J. Zhu, 2000: Use of GPS/MET refraction angles in 3D variational analysis. *Quart. J. Roy. Meteor. Soc.,* **126,** 3013–3040.